Main Chain and Side Chain Dynamics of Oxidized Flavodoxin from *Cyanobacterium anabaena*†

Weixia Liu, Peter F. Flynn, Ernesto J. Fuentes, James K. Kranz, Margaret McCormick, and A. Joshua Wand*

The Johnson Research Foundation and Department of Biochemistry and Biophysics, University of Pennsylvania, Philadelphia, Pennsylvania 19104

Received May 24, 2001; Revised Manuscript Received September 12, 2001

ABSTRACT: Oxidized flavodoxin from *Cyanobacterium anabaena* PCC 7119 is used as a model system to investigate the fast internal dynamics of a flavin-bearing protein. Virtually complete backbone and side chain resonance NMR assignments of an oxidized flavodoxin point mutant (C55A) have been determined. Backbone and side chain dynamics in flavodoxin (C55A) were investigated using ^{15}N amide and deuterium methyl NMR relaxation methods. The squared generalized order parameters (S_{NH}^2) for backbone amide N−H bonds are found to be uniformly high ($\langle S_{NH}^2 \rangle \sim 0.923$ over 109 residues in regular secondary structure), indicating considerable restriction of motion in the backbone of the protein. In contrast, methyl-bearing side chains are considerably heterogeneous in their amplitude of motion, as indicated by obtained symmetry axis squared generalized order parameters (S_{axis}^2). However, in comparison to nonprosthetic group-bearing proteins studied with these NMR relaxation methods, the side chains of oxidized flavodoxin are unusually rigid.

Flavodoxins function as soluble electron carriers between redox proteins and contain a noncovalently bound flavin mononucleotide cofactor (FMN)[1] that serves as a redox center (*1*). In the holo form of flavodoxin, the FMN molecule can exist in three distinct redox states: the oxidized flavoquinone, the one-electron-reduced flavosemiquinone, and the two-electron-reduced flavohydroquinone. The family of flavodoxins display a large range of redox potentials that vary from −50 to −260 mV for the oxidized/semiquinone redox couple and from −172 to approximately −400 mV or lower for the semiquinone/hydroquinone redox couple (*2*, *3*). The midpoint redox potentials for wild-type *Cyanobacterium anabaena* flavodoxin have been determined to be −212 and −436 mV (*4*). This compares to the corresponding midpoint potentials of −238 and −172 mV obtained for free flavin in water (*5*), indicating a significant role for the association with the protein in modulating the redox potential in this particular flavodoxin.

Flavodoxin structures are characterized by an α/β doubly wound topology, which consists of a five-stranded parallel β-sheet surrounded by α-helices on both sides (*6*) (Figure 1). The flavodoxin investigated in this study is encoded by the *nifJ* gene in the major nif-gene cluster of *C. anabaena* PCC 7119 (strain ATCC 29151) and is a polypeptide consisting of 170 amino acid residues ($M_r \sim 20$ kDa). Crystal structures have been determined for flavodoxin from *C. anabaena* in its holo (*7*) and apo forms (*8*, *9*). Comparison of these states reveals that they have minor structural differences in the immediate vicinity of the FMN binding region, including reorganization of a surface loop formed by Trp58−Leu63. This reorganization allows the indole ring of Trp58 to partially fill the cavity occupied in the holoprotein by the isoalloxazine ring of FMN (*8*). Crystal structures have been also reported for the flavodoxins from *Clostridium* MP (*10*) and *Desulfovibrio vulgaris* (*11*) in the three FMN oxidation states. Comparison of the structures determined from the different species reveals small differences in the FMN binding site, and these have been associated with observed differences in the redox potentials.

Here we are focusing on the dynamics of the oxidized state of the holoprotein and employ NMR relaxation methods to characterize the fast dynamics of both the main chain and methyl-bearing side chains. Solution NMR relaxation methods have proven to be especially useful in this regard and have revealed that proteins lacking prosthetic groups are unexpectedly dynamic, and heterogeneously so (*12*−*16*). In somewhat ironic contrast, a recent study of the internal dynamics of cytochrome c_2 revealed that this heme-binding protein is remarkably rigid. This raises the question of whether the presence of large inflexible prosthetic groups,

† Supported by NIH Grant GM35940 and equipment grants from the NIH and the ARO.

* To whom correspondence should be addressed: Department of Biochemistry and Biophysics, University of Pennsylvania, Philadelphia, PA 19104. Phone: (215) 573-7288. Fax: (215) 573-7290. E-mail: wand@mail.med.upenn.edu.

[1] Abbreviations: CPMG, Carr−Purcell−Meiboom−Gill; EDTA, ethylenediaminetetraacetate; FMN, riboflavin 5′-monophosphate; HSQC, heteronuclear single-quantum coherence; I_zC_z, two-spin longitudinal proton and carbon coherence; $I_zC_zD_z$, three-spin longitudinal proton, carbon, and deuterium coherence; $I_zC_zD_y$, three-spin longitudinal proton and carbon coherence with transverse deuterium coherence; NMR, nuclear magnetic resonance; NOE, nuclear Overhauser effect; PCR, polymerase chain reaction; pH*, pH meter reading uncorrected for the isotope effect; S_{NH}^2, squared generalized order parameter of an amide N−H bond vector; S_{axis}^2, S^2 for the symmetry axis of a methyl group; T_1, longitudinal or spin−lattice relaxation time constant; T_2, transverse or spin−spin relaxation time constant; τ_m, overall molecular tumbling correlation time; τ_e, effective correlation time for internal motion; TPPI, time-proportional phase incrementation; Tris-HCl, tris(hydroxymethyl)-aminomethane-HCl.

10.1021/bi011073d CCC: $20.00
Published on Web 11/10/2001

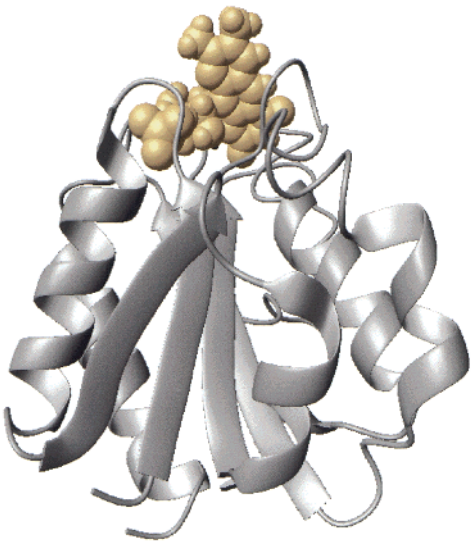

FIGURE 1: Ribbon representation of the topology of the crystal structure of oxidized *C. anabaena* flavodoxin (PDB entry 1FLV). Flavodoxin is composed of a five-stranded parallel β-sheet with flanking α-helices. The β-strands are defined as follows: strand 1, valine 31 to valine 37; strand 2, isoleucine 5 to glycine 10; strand 3, glutamine 49 to alanine 55; strand 4, lysine 82 to phenylalanine 87; and strand 5, lysine 116 to valine 118 together with leucine 142 to leucine 144. The helices are defined as follows: helix 1, glycine 14 to phenylalanine 27; helix 2 (3_{10}), glutamine 41 to asparagine 47; helix 3, tyrosine 71 to valine 77; helix 4, asparagine 101 to serine 111; and helix 5, threonine 153 to glutamine 167. The figure was prepared with the program MolMol (*67*).

such as heme or flavin, generally suppresses the larger-amplitude internal dynamics associated with proteins without such moieties intimately associated with their structure. In a first step toward answering this question for flavin-binding proteins, we report here a detailed study of the fast internal dynamics of the main chain and methyl-bearing side chains of the oxidized state of the flavodoxin.

EXPERIMENTAL PROCEDURES

Strains and Plasmids. Genomic DNA was extracted and purified using the standard protocol of the QIAGEN DNeasy Tissue kit. The *nifJ* structure gene encoding flavodoxin in the blue green algae *C. anabaena* (strain ATCC 29151) was recovered using a standard PCR overlap extension procedure and closely followed the work of Fillat et al. (*17*). The *Nde*I and *Bam*HI restriction sites of the expression vector *pET-11a* (Novagen) were introduced using the oligonucleotide coding strand primer (5′-GAATTCCATATGTCAAAGAAAATTGGTTTATTCTACGG-3′) and the anticoding strand primer (5′-CGCGGATCCTTATTACAAACCAAATTCAGACTTTAATTG-3′). Site-directed mutagenesis of pET-11a was performed using two sequential PCR reactions with the following coding strand primers: 5′-GAATTCCATATGTCAAAGAAAATTGGTTTATTCTACGG-3′ (A), 5′-CGCGGATCCTTATTACAAACCAAATTCAGACTTTAATTG-3′ (B), 5′-CAATATTTGATTATTGGCGCGCCTACTTGGAATATTG-3′ (C), and 5′-CAATATTCCAAGTAGGCGCGCCAATAATCAAATATTG-3′ (D). PCR reaction products were identified and isolated by agarose gel electrophorosis and purified using the QIAEX II gel extraction kit (QIAGEN), digested with *Nde*I and *Bam*HI, and ligated into pET-11a. Both wild-type and mutant sequences were confirmed by standard sequencing procedures.

Expression and Purification of Flavodoxin. Uniformly ^{15}N-labeled or ^{15}N- and ^{13}C-labeled proteins were produced by induction of *Escherichia coli* BL21(DE3) cells harboring the pET-11a expression vector for flavodoxin for 4 h at 37 °C during growth on minimal medium containing 1.0 g/L $^{15}NH_4Cl$, 12.8 g/L Na_2HPO_4, 3 g/L KH_2PO_4, 0.5 g/L NaCl, 2 mM $MgSO_4$, 0.1 mM $CaCl_2$, 10 μM $FeCl_2$, 5 mg/L thiamine, 2 g/L [$^{12}C_6$]- or [$^{13}C_6$]-D-glucose (Isotec), 50 mg/L ampicillin (Sigma), and 20 mg/L isopropyl β-D-thiogalactopyranoside. Triply labeled flavodoxin was prepared in a manner similar to that of the doubly labeled protein except that the medium was prepared with a H_2O:D_2O ratio of 2:3 (v/v). This gave a suitable methyl isotopomer distribution (45−50% CH_2D). Expressed flavodoxins were purified using a slightly modified version of a previously published protocol (*18*, *19*). Cells were harvested by centrifugation, washed with 10 mM Tris buffer (pH 8) containing 25 mM EDTA, and resuspended in the 10 mM Tris buffer (pH 8) containing 25 mM EDTA, 1 mM 2-mercaptoethanol, and 50 μg/mL phenylmethanesulfonyl fluoride. After one freeze−thaw cycle, the cells were treated with 0.5 mg/mL hen egg lysozyme for 30 min with stirring at room temperature followed by sonication. Unbroken cells and cellular debris were removed by low-speed centrifugation at 4 °C. The supernatant was made 50 μM in flavin mononucleotide (FMN) and gently stirred in the dark at room temperature for 2 h. The holo form of flavodoxin was further purified by chromatography on diethylaminoethylcellulose and Source 15Q ion exchange medium (Pharmacia). Both columns were equilibrated with 50 mM Tris buffer (pH 8), washed with 100 mM sodium acetate (pH 5), and eluted with a linear salt gradient of 0 to 0.5 M sodium chloride containing 100 mM sodium acetate (pH 5). The eluted flavodoxin protein was concentrated and exchanged by ultrafiltration into 100 mM potassium phosphate buffer (pH 5.8) containing 1 mM dithiotreitol. Each flavodoxin preparation was >95% pure as judged by SDS−polyacrylamide gel electrophoresis. Protein concentrations were determined spectrophotometrically on the basis of previously reported extinction coefficients for the apoprotein and holoproteins (*20*). NMR samples (650 μL) of uniformly ^{15}N-labeled flavodoxin (1 mM), uniformly ^{15}N- and ^{13}C-labeled flavodoxin (1.2 mM), or uniformly ^{15}N- and ^{13}C-labeled and random fractionally deuterated flavodoxin (1 mM) were prepared by buffer exchange and concentration via ultrafiltration and lyophilization, as required, into 100 mM potassium phosphate buffer (pH* 5.8) (95% H_2O/5% D_2O) containing 0.01% azide.

General NMR Spectroscopy. NMR spectra were recorded at 308 K on Varian INOVA 750 MHz, Varian INOVA 600 MHz, and Varian INOVA 500 MHz NMR spectrometers equipped with four RF channels, a pulsed field gradient accessory, and either a Nalorac HCN triple-resonance 750 MHz, 5 mm inverse probe with a *z*-gradient coil or Varian 500 and 600 MHz triple-resonance 5 mm inverse probes with an *x*,*y*,*z*-axes gradient coil. Presaturation of the water signal was employed during the 1.5 s relaxation delay period for the non-gradient-enhanced NMR experiments. No presaturation was used during the relaxation delay period in the gradient-enhanced experiments. ^{15}N decoupling during acquisition was accomplished using the GARP1 sequence (*21*). The ^{1}H carrier frequency was positioned at the water resonance during the experiments, unless otherwise stated.

The ^{15}N carrier position was at 119 ppm. Depending on the experiment, the ^{13}C carrier was placed in the middle of the C_α region (at 58 ppm), in the middle of the carbonyl region (at 176 ppm), or in the middle of the C_α/C_β region (at 43 ppm). Quadrature detection in indirect dimensions was accomplished using the States−TPPI method (*22*) for the non-gradient-enhanced experiments, whereas for the gradient-enhanced experiments, this was obtained by alternate N- and P-type selection for each sensitivity-enhanced indirect dimension (*23*−*25*). Sequential assignments of backbone ^1H, $^{13}C_\alpha$, $^{13}C_\beta$, and ^{15}N resonances were obtained using the HNCACB (*26*) experiment in combination with the CBCA(CO)NH (*27*) experiment. Backbone connectivities were verified using the ct-HNCO (*28*, *29*) experiment in combination with ct-HN(CA)CO (*30*). A large fraction of side chain methyl groups in flavodoxin are assigned using three-dimensional CCCTOCSY (*31*), HCCHTOCSY (*32*), and $HCCH_3$-TOCSY (*33*). In the CCCTOCSY and HCCH-TOCSY experiments, the spectral widths were 10 400 Hz in the ^1H dimension and 7500 Hz in the ^{13}C dimension. The proton carrier frequencies in the indirectly detected dimensions were positioned at 3.0 ppm. A three-dimensional methyl ^{13}C-separated $HCCH_3$-TOCSY spectra experiment was carried out using a spectral width of 5000 Hz in the ^1H dimension, 9650 Hz in the ^{13}C dimension, or 2950 Hz in the methyl ^{13}C dimension (11.7 T). The proton carrier frequency was positioned at 2.1 ppm, and the ^{13}C methyl carrier frequency was positioned at 18.2 ppm. Stereospecific assignments of the methyl groups of leucine and valine were obtained using the limited glucose labeling approach of Neri et al. (*34*).

Data Processing and Analysis. NMR data were processed on Silicon Graphics Indigo O2 workstations using Felix version 98 (Molecular Simulations Inc., San Diego, CA). Free induction decays in the acquisition dimension were multiplied by a Gaussian function and zero-filled to 1024 complex points prior to Fourier transformation. In all indirect dimensions, data were apodized using a 90° shifted sine-bell squared window function and zero-filled to the next power of 2 prior to Fourier transformation. The pH-corrected values are reported here in parts per million relative to DSS. ^{15}N and ^{13}C chemical shifts were referenced indirectly using the consensus X_i ratios of gyromagnetic ratios [0.101 329 118 and 0.251 449 528 for $^{15}N/^1H$ and $^{13}C/^1H$, respectively (*35*)].

NMR Relaxation Experiments. ^{15}N longitudinal (T_1) and transverse (T_2) relaxation rates were measured at 11.7 and 14.1 T, corresponding to ^{15}N Larmor frequencies of 50.6 and 60.9 MHz, respectively, using a pulse sequence based on the ^{15}N HSQC experiment (*36*−*40*). The $\{^1H\}-^{15}N$ NOE was also measured at 11.7 and 14.1 T, based on a $^1H-^{15}N$ correlation experiment recorded with and without broadband ^1H saturation that produces a change in the intensity of $^1H-^{15}N$ cross-peaks due to the nuclear Overhauser effect (*41*). The experiment designed to measure longitudinal relaxation employed a cycling scheme based on the Freeman−Hill approach wherein signal intensities vary from unity to zero (*42*). Cross-correlated relaxation during longitudinal relaxation was eliminated by applying 120° ^1H pulses every 5 ms. Cross-correlation effects during transverse relaxation were eliminated by applying ^{15}N 180° pulses in the CPMG train every 900 μs and by applying ^1H 180° pulses that were centered in the CPMG module (*43*). Standard ^{15}N relaxation experiments (*39*) were employed to measure the ^{15}N T_1, T_2, and NOE values of amide nitrogens. Each of the three experiments was conducted at field strengths of 11.7 and 14.1 T. Relaxation decays for these coherences were sampled at identical time points at the two field strengths. The ^{15}N T_1 relaxation time points were 50, 90*, 135, 207*, 290, 380, 480, 586*, and 700 ms; the ^{15}N T_2 time points were 7.8*, 15.5, 23.3, 31.0*, 46.5, 62.0, 77.5, 101*, and 124 ms. Asterisks indicate duplicate points.

Deuterium Relaxation Experiments for Side Chain Dynamics. Deuterium relaxation experiments assessed relaxation of multiple-spin coherences involving longitudinal proton and carbon coherence [$R(I_zC_z)$], longitudinal proton, carbon, and deuterium coherence [$R(I_zC_zD_z)$], and longitudinal proton, carbon nuclei with transverse deuterium coherence [$R(I_zC_zD_y)$] generated within each methyl group (*12*). Each of the three experiments was conducted at field strengths of 11.7 and 14.1 T. The I_zC_z relaxation time points were 1.0*, 11.2, 22.4, 33.6*, 44.8, 56.0, 67.2, 78.5*, and 90.0 ms. The $I_zC_zD_z$ time points were 3.7*, 10.5, 19.2, 29.6, 41.4, 54.4, 68.5*, and 83.7 ms. The $I_zC_zD_y$ time points were 0.9, 2.6*, 4.7, 7.4*, 10.4, 13.6, 17.1, 21.0*, and 25.0 ms. Asterisks indicate duplicate points. All deuterium relaxation data were fitted to a single exponential as described previously.

Relaxation Data Analysis. The ^{15}N and ^2H relaxation data were analyzed using the Lipari−Szabo model-free formalism (*44*, *45*). An effective N−H bond length of 1.04 Å (*46*) and a quadrapolar coupling constant of 165 kHz (*47*) were employed. Overall rotational correlation times were determined for flavodoxin based on ^{15}N T_1, T_2, and NOE measurements at 11.7 and 14.1 T using the grid search method of Dellwo and Wand (*48*). Cross-peak intensities were used to quantify relaxation, and the uncertainties in these intensities were estimated from duplicate measurements and the root-mean-square noise level of the spectrum base plane. The residual χ^2 values were generally less than or equal to the number of fitted time versus intensity points that suggest the data were well fit.

RESULTS

Recombinant Flavodoxin. Purified recombinant wild-type flavodoxin was found by polyacrylamide gel electrophoresis to exist as a dimer, presumably due to formation of an intermolecular disulfide bridge between the single cysteine of wild-type flavodoxin (*49*). To avoid complications in the NMR analysis, we created a C55A mutant protein. The flavodoxin (C55A) mutant shows a single band by electrophoresis, consistent with the monomeric form of the protein. This mutant has been created previously in the highly homologous flavodoxin from *Azotobacter vinelandii* and found to have redox and physical properties essentially identical to those of the wild-type protein (*49*). The C55A mutant form of flavodoxin was used exclusively in the relaxation studies described here.

Backbone Assignments of Flavodoxin (C55A). Sequential assignments of backbone ^1H, $^{13}C_\alpha$, $^{13}C_\beta$, and ^{15}N resonances were obtained using the HNCACB (*26*) and CBCA(CO)-NH (*27*) three-dimensional spectra. Backbone connectivities were verified by reference to ct-HNCO (*28*, *29*) and ct-HN-(CA)CO (*30*) spectra. Starting from the published partial assignments of the wild-type protein (*50*, *51*), we were able

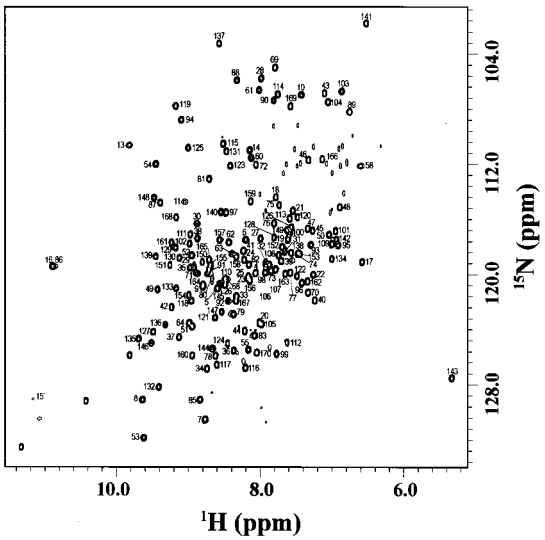

FIGURE 2: First ^{15}N HSQC plane from a ^{15}N T_1 three-dimensional data set recorded for ^{15}N-labeled recombinant oxidized *C. anabaena* flavodoxin (C55A) obtained at 14.1 T and 308 K. The residue-specific assignments of backbone amide N−H corrections are indicated.

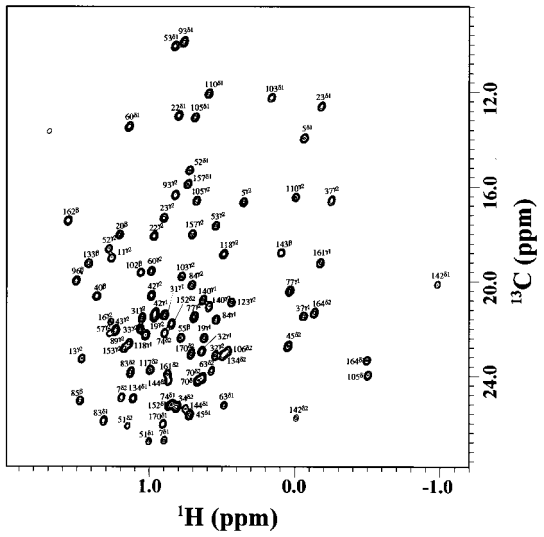

FIGURE 3: ^{13}C HSQC plane from a ^{13}C $I_zC_zD_y$ three-dimensional data set recorded for ^{2}H-, ^{13}C-, and ^{15}N-labeled recombinant oxidized *C. anabaena* flavodoxin (C55A) obtained at 14.1 T and 308 K. The residue-specific assignments of side chain methyl corrections are indicated.

to obtain virtually complete backbone $^{1}H_N$, $^{13}C_\alpha$, $^{13}C_\beta$, and ^{15}N resonance assignments of flavodoxin. Some cross-peaks have much weaker intensities than the bulk of the resonances found in the ^{15}N HSQC spectra. These weaker cross-peaks are located in the assignment discontinuities, i.e., in the sequence between residues 55−57 and 63−67. This strongly suggests conformational heterogeneity and flexibility on the millisecond to microsecond time scale in this region of flavodoxin. The ^{15}N resonance assignments are summarized in Figure 2.

Assignments of Flavodoxin (C55A) Methyl Side Chains. The side chain methyl groups in flavodoxin were assigned using the three-dimensional CCC-TOCSY (*31*), HCCH-TOCSY (*32*), and HCCH$_3$-TOCSY (*33*) experiments. The methyl ^{13}C-separated three-dimensional HCCH$_3$-TOCSY experiment takes advantage of the inherently good separation of methyl cross-peaks in proton−carbon correlated spectra, and it has high digital resolution in the methyl carbon dimension. Stereospecific isopropyl methyl assignments were determined using the method of Neri et al. (*34*), which allowed the assignment of 20 of 20 valine and 29 of 30 leucine prochiral methyl pairs. In all, 90 of the 92 methyls present in the protein were stereospecifically assigned. The methyl resonance assignments are summarized in Figure 3.

Characterization of Molecular Tumbling. As a prelude to the study of dynamics based on NMR relaxation, the global tumbling of the protein must be characterized. The influence of anisotropic tumbling on model-free parameters (*44, 45*) derived from NMR relaxation has been extensively documented (*40, 52, 53*). To characterize global tumbling of flavodoxin, we have employed a standard strategy that has been outlined in detail elsewhere (*15, 54*). Using ^{15}N NMR relaxation parameters (T_1, T_2, and NOE) obtained at two magnetic field strengths (11.7 and 14.1 T), the isotropic global tumbling time (τ_m) was determined using a grid-based search method (*48*) to be 6.35 ns. The rotational anisotropy expressed as the ratio of diffusion coefficients parallel and perpendicular to the principal axis of the rotational diffusion tension ($D_{||}/D_\perp$) was found to be 0.93, with the θ and ϕ angles

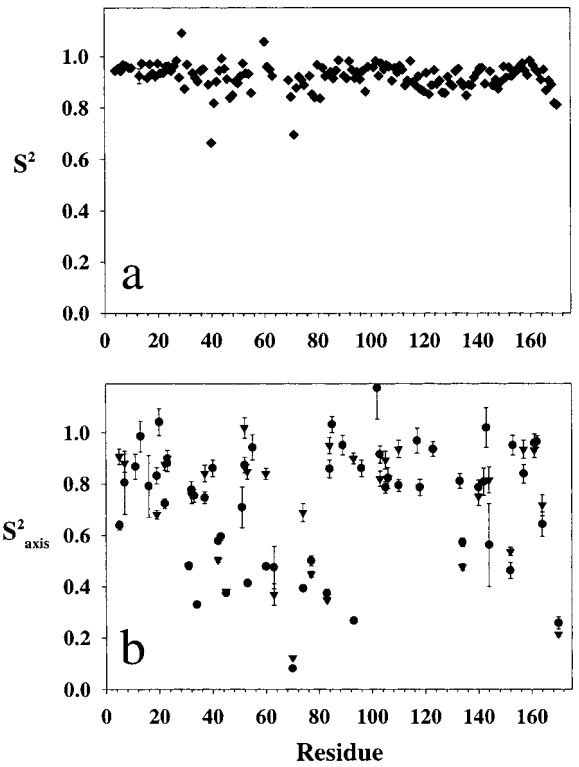

FIGURE 4: Squared generalized order parameters for backbone amide N−H (S_{NH}^2) (a) and methyl symmetry axis squared generalized order parameters (S_{axis}^2) for methyl-bearing amino acids (b) of recombinant oxidized *C. anabaena* flavodoxin (C55A).

equal 1.22 and 1.89 rad, respectively. This small anisotropy may be neglected, and the simple isotropic global tumbling form of the spectral density was employed in the subsequent analysis using a value for τ_m of 6.35 ns.

Backbone Dynamics of Flavodoxin (C55A). The range of values of squared generalized order parameters for backbone amide N−H bond vectors (S_{NH}^2) of flavodoxin (C55A) is summarized in Figure 4. As has been observed for most proteins, the S_{NH}^2 parameters for residues located in regular

Table 1: Squared Generalized Order Parameters of Amide N−H Groups of Oxidized Flavodoxin (C55A) Obtained at 35 °C

residue	S^2	σ	τ_e (ps)	σ	residue	S^2	σ	τ_e (ps)	σ	residue	S^2	σ	τ_e (ps)	σ	residue	S^2	σ	τ_e (ps)	σ
K4	0.943	0.012	83	136	D47	0.838	0.004	61	3.3	Y95	0.939	0.009	0.0	0.0	A133	0.952	0.007	79	26
I5	0.951	0.008	0.0	0.0	Y48	0.849	0.005	13	3.2	A96	0.910	0.006	0.4	1.4	L134	0.900	0.005	14	5.0
G6	0.942	0.007	1.3	3.5	Q49	0.901	0.009	11	7.6	D97	0.943	0.008	0.1	1.1	R135	0.885	0.009	19	6.2
L7	0.966	0.008	0.9	6.3	Y50	0.896	0.007	36	6.8	N98	0.863	0.005	21	3.6	N136	0.848	0.013	7.9	4.8
F8	0.962	0.009	0.1	0.7	L51	0.922	0.007	14	8.6	F99	0.959	0.008	0.0	0.0	G137	0.889	0.007	7.5	4.7
Y9	0.956	0.005	0.0	0.0	I52	0.972	0.006	0.0	0.0	Q100	1.012	0.217	nd[a]	nd[a]	K138	0.886	0.005	9.9	4.3
G10	0.954	0.011	8.4	16	I53	0.934	0.010	18	14	D101	0.957	0.005	58	17	F139	0.917	0.007	0.2	1.3
T13	0.923	0.029	95	257	G54	0.931	0.009	0.3	2.1	A102	0.982	0.007	33	39	V140	0.934	0.007	0.1	1.0
G14	0.972	0.010	0.2	2.6	C55	0.858	0.007	5.9	3.9	I103	0.924	0.010	0.0	0.0	G141	0.953	0.007	0.0	0.0
T16	0.915	0.009	0.0	0.2	I60	1.057	0.013	13	15	G104	0.973	0.007	15	53	L142	0.955	0.007	35	17
E17	0.969	0.007	0.0	0.5	G61	0.960	0.010	57	39	I105	0.949	0.007	29	15	A143	0.892	0.008	23	6.5
S18	0.933	0.006	0.1	0.9	E62	0.949	0.006	2.4	4.7	L106	0.966	0.006	0.3	2.6	D145	0.941	0.006	0.3	1.5
V19	0.921	0.008	0.0	0.2	L63	0.923	0.007	28	16	E107	0.959	0.006	0.1	0.9	E146	0.887	0.014	0.1	1.0
A20	0.972	0.005	47	25	G69	0.907	0.006	25	6.5	E108	0.904	0.007	9.5	6.8	D147	0.908	0.010	0.3	1.6
E21	0.934	0.005	0.1	0.9	L70	0.842	0.005	67	4.3	K109	0.955	0.006	32	13	N148	0.873	0.011	0.1	0.7
I22	0.934	0.009	36	11	Y71	0.695	0.004	107	2.6	I110	0.936	0.009	15	9.3	Q149	0.900	0.009	1.7	3.0
I23	0.960	0.004	0.0	0.0	S72	0.877	0.005	79	5.7	S111	0.963	0.006	3.7	7.3	S150	0.960	0.006	0.0	0.0
R24	0.962	0.006	1.5	4.9	E73	0.921	0.008	23	8.8	Q112	0.947	0.005	10	8.6	D151	0.917	0.005	50	7.8
D25	0.943	0.004	0.0	0.2	L74	0.908	0.005	16	5.5	R113	0.887	0.006	19	4.9	L152	0.957	0.008	0.3	2.2
E26	0.962	0.005	3.9	7.1	D75	0.888	0.005	48	5.1	G114	0.906	0.007	2.6	3.6	T153	0.922	0.009	0.0	0.0
F27	0.983	0.009	2.9	34	D76	1.025	0.207	nd[a]	nd[a]	G115	0.982	0.008	1.9	7.8	D154	0.939	0.005	59	10
G28	0.917	0.008	39	10	V77	0.924	0.006	2.1	4.3	K116	0.900	0.006	4.8	5.0	D155	0.943	0.005	7.7	7.9
N29	1.091	0.010	0.0	0.0	D78	0.853	0.005	45	4.2	T117	0.886	0.006	23	4.8	R156	0.959	0.005	19	11
D30	0.873	0.005	69	5.1	F79	0.840	0.007	52	4.9	V118	0.922	0.012	0.5	2.6	I157	0.973	0.010	140	511
V31	0.968	0.005	152	30	N80	0.967	0.006	1.6	5.5	G119	0.870	0.007	22	4.8	K158	0.944	0.005	9.7	8.2
V32	nd[a]	nd[a]	nd[a]	nd[a]	G81	0.836	0.006	48	4.2	Y120	0.864	0.005	0.0	0.0	S159	0.926	0.005	0.0	0.0
T33	0.935	0.008	18	12	K82	0.955	0.007	0.2	1.6	W121	0.935	0.009	8.4	9.2	W160	0.984	0.006	0.9	5.3
L34	0.916	0.006	15	7.6	L83	0.922	0.007	12	8.3	S122	0.852	0.005	0.0	0.0	V161	0.965	0.007	7.6	14
H35	0.903	0.009	6.9	6.7	V84	0.930	0.007	38	11	T123	0.888	0.013	0.0	0.2	A162	0.948	0.005	26	9.0
D36	0.943	0.010	2.9	6.4	A85	0.940	0.009	14	13	D124	0.946	0.005	0.0	0.0	Q163	0.938	0.007	6.2	7.3
V37	0.950	0.007	1.6	4.5	Y86	0.913	0.010	0.0	0.0	G125	0.892	0.008	0.1	0.9	L164	0.909	0.010	0.0	0.2
Q39	0.890	0.006	15	5.7	F87	0.945	0.008	12	11	Y126	0.905	0.007	0.0	0.0	K165	0.948	0.005	10	9.3
A40	0.664	0.003	20	0.9	G88	0.985	0.012	52	329	D127	0.859	0.007	1.3	2.1	S166	0.867	0.004	6.0	3.1
E41	0.818	0.005	23	3.1	G90	0.924	0.010	0.2	1.5	F128	0.857	0.005	0.5	1.1	E167	0.905	0.006	41	6.8
V42	0.902	0.004	33	5.0	D91	0.913	0.004	62	6.4	N129	0.920	0.009	0.0	0.0	F168	0.890	0.006	18	5.2
T43	0.944	0.004	73	12	Q92	0.981	0.009	43	323	D130	0.893	0.007	3.3	3.8	G169	0.818	0.005	37	2.9
D44	0.992	0.007	229	165	I93	0.947	0.009	0.4	2.7	S131	0.884	0.005	0.0	0.0	L170	0.811	0.004	51	2.8
L45	0.951	0.005	0.0	0.0	G94	0.915	0.009	0.0	0.0	K132	0.942	0.009	2.9	5.8					
N46	0.912	0.005	44	5.9															

[a] Not determined.

secondary structures are generally high, with an average 0.923 for the 109 residues in regular secondary structure as defined by analysis of the crystal structure of the protein (*7*). Analysis of the results obtained by Wagner and coworkers (*55*) indicates a similar degree of rigidity for oxidized flavodoxin from *Anacystis nidulans* ($\langle S_{NH}^2 \rangle \sim 0.89$). Most of the amide groups that have high S_{NH}^2 values also have fitted τ_e values approaching zero, indicating the presence of extremely fast and highly restricted motion (Table 1). A few sites have best fit S_{NH}^2 values closely approaching and sometimes exceeding the theoretical limit of unity. Generally, those sites having order parameters greater than unity exceed the theoretical limit by less than the fitted precision, and this apparent discrepancy can be quite reasonably ascribed to simple experimental error at an unusually rigid site.

Side Chain Dynamics of Flavodoxin (C55A). Relaxation rates of I_zC_z, $I_zC_zD_z$, and $I_zC_zD_y$ coherences were measured at static magnetic field strengths of 11.7 and 14.1 T and 308 K for $^{13}CH_2D$ isotopomers from 90 methyl groups in flavodoxin (C55A). Methyl symmetry axis squared generalized order parameters (S_{axis}^2) values were determined in the usual way (*54*) with an in-house computer program implementing a grid-based solution to the model-free equations (*48*). Methyl symmetry axis order parameters were obtained under the assumption of tetrahedral methyl geometry. The S_{axis}^2 parameters of methyl groups in the side chains of flavodoxin (C55A) vary substantially, from ~0.1 to ~1 (Figure 4). The corresponding τ_e values also show considerable heterogeneity ranging from 7 to ~100 ps (Table 2). A color-coded representation of the side chain dynamics of flavodoxin (C55A) is presented in Figure 5. The S_{axis}^2 values are color-coded and mapped onto individual methyl groups in the three-dimensional crystal structure of flavodoxin. There is an apparent clustering of both large-amplitude and small-amplitude methyl-bearing side chain motions in flavodoxin (C55A). For example, the methyl groups with the lowest S_{axis}^2 values [δ1 (0.081) and δ2 (0.123) of leucine 70] lie in a β-turn between β-strand 3 and helix 3, and appear to form a cluster with a group of methyl groups that lie between helices 2 and 3 and also have low to intermediate S_{axis}^2 values (see Figures 4 and 5). This region includes γ1 (0.578) and γ2 (0.505) of valine 42, γ2 (0.595) of threonine 43, δ1 (0.375) and δ2 (0.382) of leucine 45, δ1 (0.394) and δ2 (0.689) of leucine 74, and γ1 (0.501) and γ2 (0.449) of valine 77.

Regions of exceptionally high rigidity are also apparent. The methyl groups of residues lying between helices 1 and 5 are uniformly high and form a ridge of ordered methyl side chains. These groups include γ2 (0.791) of threonine

Table 2: Squared Generalized Order Parameters for Methyl Group Symmetry Axes of Methyl-Bearing Amino Acid Side Chains of Oxidized Flavodoxin (C55A) Obtained at 35 °C

residue	S_{axis}^2	σ	τ_e (ps)	σ	χ^2	residue	S_{axis}^2	σ	τ_e (ps)	σ	χ^2
I5 δ1	0.638	0.018	10	1	1.1	V77 γ2	0.449	0.012	53	1	0.1
I5 γ2	0.907	0.030	22	2	2.1	L83 δ1	0.374	0.018	38	2	2.3
L7 δ1	0.805	0.123	53	14	0.3	L83 δ2	0.348	0.008	22	1	3.1
L7 δ2	0.881	0.036	12	2	2.7	V84 γ1	0.859	0.035	43	3	1.2
T11 γ2	0.867	0.121	35	10	1.9	V84 γ2	0.950	0.032	24	2	5.3
T13 γ2	0.985	0.060	56	6	0.1	A85 β	1.032	0.032	16	2	9.3
T16 γ2	0.791	0.043	27	3	0.9	T89 γ2	0.951	0.049	45	4	3.1
V19 γ1	0.832	0.032	38	3	0.7	I93 δ1	0.268	0.007	38	1	12.7
V19 γ2	0.681	0.017	29	1	14.4	I93 γ2	0.899	0.021	27	1	2.7
A20 β	1.042	0.052	64	5	1.4	A96 β	0.861	0.032	68	3	7.5
I22 δ1	0.723	0.018	14	1	3.5	A102 β	1.174	0.122	118	19	6.2
I22 γ2	0.876	0.023	34	2	2.7	I103 δ1	0.915	0.034	7.2	2	4.2
I23 δ1	0.881	0.033	8.5	2	7.0	I103 γ2	0.820	0.03	22	2	0.5
I23 γ2	0.900	0.031	29	2	1.5	I105 δ1	0.786	0.022	10	1	2.9
V31 γ1	0.481	0.014	64	2	4.1	I105 γ2	0.893	0.035	45	3	0.8
V31 γ2	0.482	0.012	39	1	4.0	L106 δ1	0.823	0.041	39	4	1.5
V32 γ1	0.777	0.033	76	4	0.0	L106 δ2	0.823	0.041	39	4	1.5
V32 γ2	0.758	0.035	46	3	2.9	I110 δ1	0.794	0.023	7.7	1	5.2
T33 γ2	0.754	0.024	67	3	13.2	I110 γ2	0.936	0.034	25	2	7.9
L34 δ2	0.330	0.012	56	2	14.7	T117 γ2	0.969	0.049	48	4	0.7
V37 γ1	0.746	0.023	25	2	3.7	V118 γ1	0.786	0.032	83	4	0.1
V37 γ2	0.841	0.032	11	2	2.1	V118 γ2	0.786	0.032	83	4	0.1
A40 β	0.861	0.032	68	3	7.5	T123 γ2	0.936	0.029	15	2	3.9
V42 γ1	0.578	0.011	33	1	17.9	A133 β	0.811	0.029	32	2	0.0
V42 γ2	0.505	0.011	57	1	13.6	L134 δ1	0.573	0.017	33	2	0.7
T43 γ2	0.595	0.014	39	1	7.0	L134 δ2	0.477	0.013	24	1	0.8
L45 δ1	0.375	0.010	33	1	1.8	V140 γ1	0.786	0.029	36	3	0.2
L45 δ2	0.382	0.009	29	1	2.0	V140 γ2	0.751	0.035	39	3	0.2
L51 δ1	0.709	0.079	52	9	0.5	L142 δ1	0.808	0.053	10	3	0.4
L51 δ2	0.709	0.079	52	9	0.5	A143 β	1.019	0.077	95	9	2.6
I52 δ1	0.874	0.031	19	2	3.1	L144 δ2	0.815	0.051	41	5	3.9
I52 γ2	1.019	0.040	19	2	6.1	L152 δ1	0.463	0.032	71	4	1.4
I53 δ1	0.415	0.013	21	1	5.1	L152 δ2	0.537	0.016	28	1	1.3
I53 γ2	0.848	0.029	16	2	1.1	T153 γ2	0.945	0.038	33	3	0.7
A55 β	0.943	0.049	65	5	1.1	I157 δ1	0.839	0.036	31	3	2.7
I60 δ1	0.479	0.011	14	1	8.5	I157 γ2	0.935	0.036	26	3	3.0
I60 γ2	0.839	0.022	8.8	1	4.2	V161 γ1	0.960	0.034	34	3	1.6
L63 δ1	0.475	0.082	79	12	2.5	V161 γ2	0.932	0.030	12	2	14.2
L63 δ2	0.370	0.042	37	4	1.1	A162 β	0.965	0.023	25	2	3.2
L70 δ1	0.081	0.004	40	1	11.7	L164 δ1	0.643	0.048	79	7	0.5
L70 δ2	0.123	0.005	37	1	19.7	L164 δ2	0.717	0.041	60	5	2.6
L74 δ1	0.394	0.011	65	2	0.4	L170 δ1	0.259	0.024	38	3	6.2
L74 δ2	0.689	0.036	30	3	7.2	L170 δ2	0.215	0.008	32	1	5.9
V77 γ1	0.501	0.020	83	3	0.9						

16, γ1 (0.832) of valine 19, β ($\sim$1) of alanine 20, δ1 (0.723) and γ2 (0.876) of isoleucine 22, δ1 (0.881) and γ2 (0.900) of isoleucine 23, γ2 (0.945) of threonine 153, δ1 (0.839) and γ2 (0.935) of isoleucine 157, γ1 (0.960) and γ2 (0.932) of valine 161, and β (0.965) of alanine-162. In addition, the base of the FMN binding pocket is lined with methyl groups that have relatively high S_{axis}^2 values. These groups fall at the ends of the β-strands of the β-sheet that composes the core of flavodoxin, and include the β-methyl ($\sim$1) of alanine 102, β ($\sim$1) of alanine 143, γ2 (0.791) of threonine 16, γ2 (0.951) of threonine 89, δ2 (0.815) of leucine 144, and γ2 (0.867) of threonine 11. These three threonines in addition to threonine 13, whose methyl group has an S_{axis}^2 of 0.985, form a coordinating network for the phosphate moiety of the FMN molecule. The dynamics of the four Trp indole rings could also be determined from the ^{15}N relaxation studies; all four are found to be relatively rigid ($\langle S_{NH}^2 \rangle = 0.798 \pm 0.034$).

The S_{axis}^2 parameters indicate substantial heterogeneity of side chain motion in flavodoxin (C55A). This heterogeneity is qualitatively consistent with similar investigations of other proteins and stands in rather remarkable contrast to the relatively limited range of backbone motion. Quantitatively, however, the internal dynamics of flavodoxin (C55A) are quite distinct from those seen in most other proteins. This is illustrated by the histogram of the distribution of S_{axis}^2 parameters shown in Figure 6. A bimodal distribution of S_{axis}^2 values is present, with the two distributions centered at S_{axis}^2 values of 0.45 and 0.85. Multimodal distributions of the amplitudes of fast internal motion in proteins have been observed previously, particularly in a recent study of the temperature dependence of side chain motion in a calmodulin−peptide complex (*16*). Retrospective analysis of side chain order parameters obtained on other proteins at individual temperatures suggests that a trimodal distribution of dynamical amplitudes may be a general property of proteins (*16*). The three distributions are centered on S_{axis}^2 values of $\sim$0.3, 0.6, and 0.85 at room temperature. In contrast, a recent study of the fast internal motion of a *c*-type cytochrome revealed the virtual absence of the high-amplitude motional class with a concomitant enrichment of the lowest-amplitude motional class (*54*). A similar bimodal, rather than trimodal, distribution of S_{axis}^2 values is seen here for flavodoxin (C55A). This bimodal distribution has a considerable relative

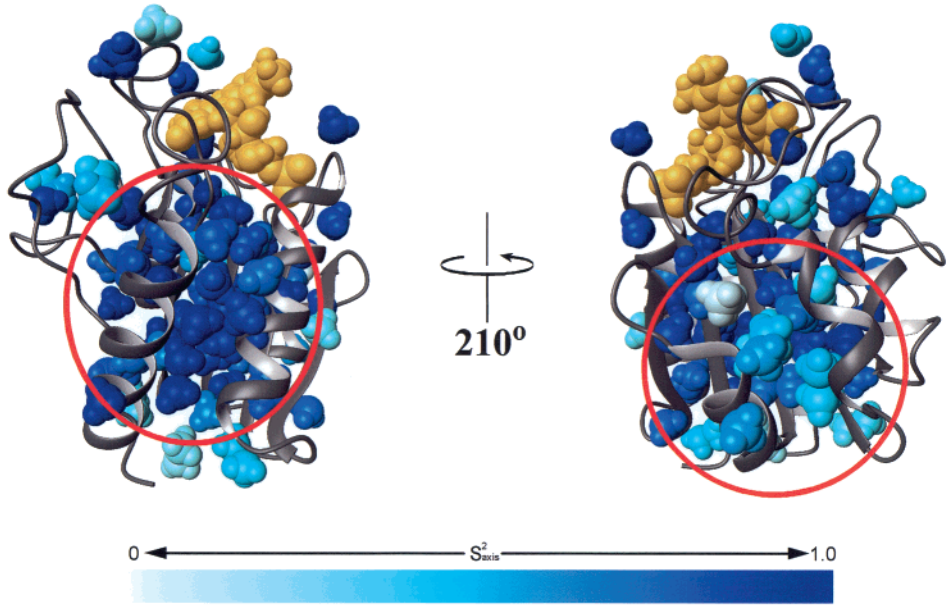

FIGURE 5: Color-coded representation of the dynamics of methyl-bearing side chains of flavodoxin C55A. S_{axis}^2 values are color-mapped onto individual methyl groups in the three-dimensional structure of flavodoxin from *C. anabaena*. Two views are shown. S_{axis}^2 values range from 0 (white) to 1 (blue) on a continuous scale as shown in the color legend at the bottom of the figure. The left view shows a cluster including the methyl groups of residues lying between helices 1 and 5 that have uniformly high S_{axis}^2 values. The right view shows a cluster with a group of methyl groups that lie between helices 2 and 3 that have low to intermediate S_{axis}^2 values. The figure was prepared with the program MolMol (*67*).

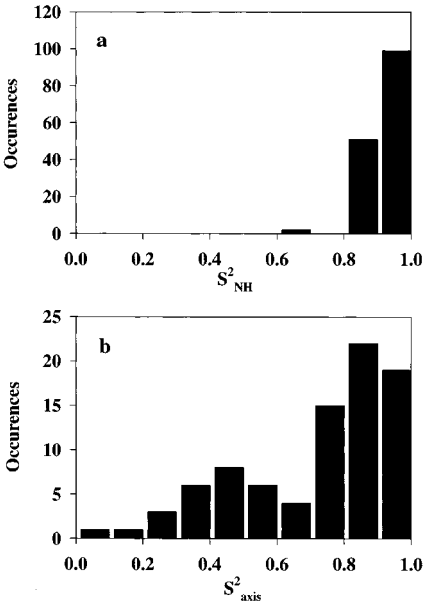

FIGURE 6: Histogram of the distribution of S_{NH}^2 (a) and S_{axis}^2 (b) parameters of recombinant *C. anabaena* flavodoxin (C55A).

enrichment of the most motionally restricted class centered on ~0.85, similar to the result obtained with cytochrome c_2 (*54*).

Stereochemical Correlates of Motional Amplitudes. The range of S_{axis}^2 values in flavodoxin (C55A) by residue type are 0.94 ± 0.09 (alanine), 0.87 ± 0.13 (threonine γ_2), 0.90 ± 0.06 (isoleucine γ_2), 0.72 ± 0.17 (valine), 0.69 ± 0.22 (isoleucine δ_1), and 0.51 ± 0.24 (leucine). The average S_{axis}^2 values for each residue type are larger than those observed for most other proteins (*12*, *15*, *56*−*60*). It appears that flavodoxin (C55A) is among the most rigid proteins examined to date.

It is reasonable that certain structural features may modulate the extent of motions possible for particular side chain elements. For example, it would seem physically plausible that the fewer the number of degrees of freedom by which a given methyl group is separated from its α-amino acid backbone, the more correlated its motion should be with the motion of its associated amide N−H group. For oxidized flavodoxin (C55A), this is clearly true for alanine, isoleucine $\gamma 2$, and threonine, less accurate for valine, and not true for leucine and isoleucine δ methyls (see Table 2).

Structural Correlates of Motional Amplitudes. We have been unable to detect a clear correlation between secondary structure and amplitude of side chain motion. However, an interesting albeit weak correlation of amplitude of motion with the depth of burial is observed. The GRASP program (*61*) was used to determine the distance between each methyl carbon or amide nitrogen and the molecular surface of the crystal structure. The dependence of the S_{NH}^2 and S_{axis}^2 parameters on the distance to the surface is shown in Figure 7. A weak but interesting correlation for both is seen. The distance from the surface becomes an increasingly dominant predictor of angular order the further the group in question is from the molecular surface. Though conceptually quite natural, this has not been noted previously. As is obvious from the figure, apparently there are other variables that influence side chain motion near the surface of the protein, but these become less important as the side chain becomes more deeply buried. It is difficult to quantify this without a model that specifies these other variables, which are unknown at this time. However, the mean and variance of the squared generalized order parameters increases and decreases, respectively, with increasing depth of burial (Table 3). There is essentially no dependence of S_{NH}^2 on the distance to the FMN surface and only the barest of hints of negative correlation of S_{axis}^2 with distance to the

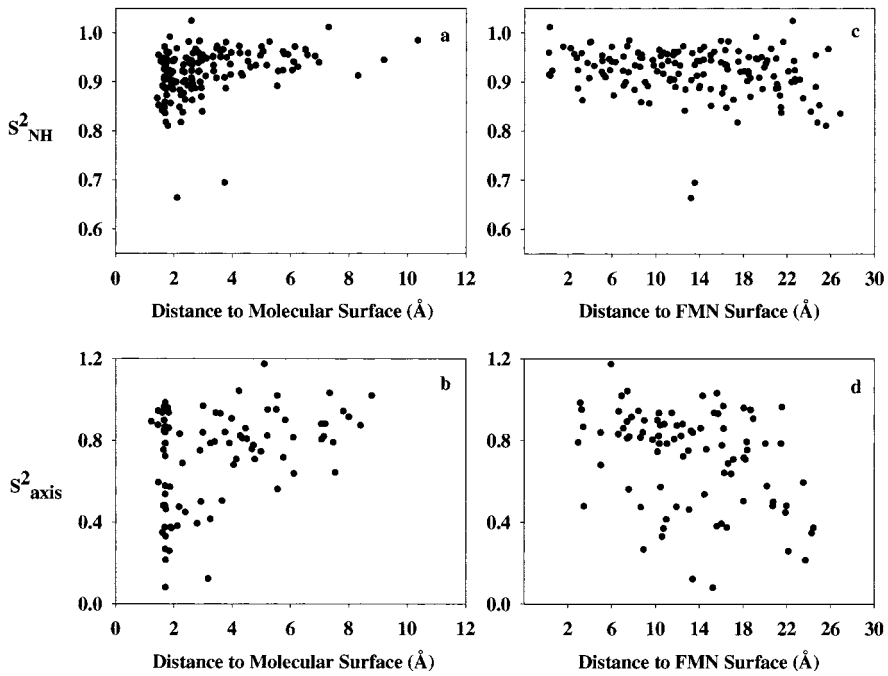

FIGURE 7: Dependence of the amplitude of fast motion on the depth of burial and distance to the FMN prosthetic group. Panels a and c show the dependence of S_{NH}^2 on the distance of the amide nitrogen from the molecular surface and from the surface of the FMN moiety, respectively. Panels b and d show the dependence of S_{axis}^2 on the distance of the methyl carbon from the molecular surface and from the surface of the FMN moiety, respectively.

Table 3: Correlation of Amplitude of Motion with Depth of Burial

amide NH			
depth of burial (Å)	1.5−2.5	2.5−3.5	3.5−4.5
average S^2	0.905	0.937	0.952
standard deviation	0.057	0.046	0.018
methyl groups			
depth of burial (Å)	1.2−2.2	3.2−4.2	5.2−6.2
average S^2	0.624	0.753	0.850
standard deviation	0.256	0.168	0.127

FMN surface (Figure 7). There is no apparent dependence of S_{NH}^2 or S_{axis}^2 on the distance to the Trp indole rings (not shown).

A similar analysis of squared generalized order parameters obtained for ubiquitin (*15*), calcium-saturated calmodulin, both free and in complex with a target domain (*62*), and cytochrome c_2 (*54*) did not reveal a similar correlation with depth of burial. This may simply reflect the fact that flavodoxin (C55A) is among the largest proteins whose side chain dynamics have been studied in detail and is hinting at a dependence that will only be fully revealed in larger proteins. Finally, in none of these cases, including flavodoxin (C55A), was a correlation of amplitude of motion with solvent accessible surface area found.

Although the bulk of the side chain methyl groups populating the core have relative high methyl symmetry axis squared generalized order parameters, buried methyl groups with lower values exist as well. Buried methyl groups exhibiting low methyl symmetry axis squared generalized order parameters have been noted frequently in previous studies (*13*, *15*, *57*−*59*).

Dynamics at the FMN−*Protein Interface.* Three segments of the flavodoxin sequence contact the FMN and contribute to the binding of the prosthetic group: phosphate binding to the loop formed by residues 11−16 and an extensive network of hydrogen bonds to the isoalloxazine ring by residues 56−63 and 89−101 (*7*). The flavin ring is also bracketed by two aromatic side chains, Tyr95 and Trp58. The influence of the FMN cofactor on side chain dynamics seems to defy simple description, as might be derived, for example, by invoking steric constraint. Certainly, as noted above, the fact that the loop segment (^{11}TQTGKT^{16}) interacts extensively with the phosphate moiety of FMN presumably accounts for the rather high S_{axis}^2 values of the γ methyls of threonine 13 and threonine 11.

DISCUSSION

Many proteins use tightly noncovalently associated or covalently attached prosthetic groups or cofactors to perform their biological function. The modulation of the chemical properties of the prosthetic group or cofactor via its association with the protein host is a common theme that is often expressed in terms of the differential affinity of the protein for one chemical state over another. This is particularly true for the flavoproteins where the bound flavin can, in principle, exist in three distinct redox states. Differential stabilization of the three redox states has as a direct consequence a significant alteration of the redox potentials of the bound FMN relative to their free solution values. The energetics of the association of FMN with the apoprotein have been dissected using a variety of approaches (*3*, *63*). These studies suggest that interaction with the phosphate provides ~7 kcal mol^{-1} to the binding free energy while interactions with the isoalloxazine ring contribute ~5 kcal mol^{-1}.

It is clear from the studies of fast main chain and side chain dynamics presented here that oxidized flavodoxin (C55A) is an unusually rigid protein and displays little of the high-amplitude dynamics normally associated with proteins lacking large prosthetic groups or cofactors (*16*). Indeed, the motional class centered on an S_{axis}^2 value of ~0.3 is virtually absent, and the class centered on an S_{axis}^2 value

of 0.6 is significantly diminished relative to proteins not having a bound prosthetic group. Considerable insight into the significance of this exceptional rigidity can be obtained from a rather simple but direct interpretation of the small-amplitude and presumably quasi-harmonic motion reported by the high squared generalized order parameters that were obtained (*64*). In this view, the relatively high order parameters correspond to the presence of very limited residual protein entropy. Interestingly, this uniform rigidity does not appear to be reflected in the hydrogen exchange behavior of holoflavodoxin from *A. vinelandii* (*65*).

A central question that is then raised is how entropic the apo state of the protein is and whether the residual entropy of the holoprotein is modulated by a change in the redox state of the flavin. It is also interesting to note that the midpoint of the oxidized/semiquinone redox couple is only moderately shifted from its usual free solution value, while the seminquinone/hydroquinone redox couple is dramatically shifted, by more than −200 mV. Thus, it will be interesting to see the dynamical consequences of the interaction of protein with the half-reduced and fully reduced states of FMN. These studies are in progress.

Analysis of results from previous studies of proteins, all of which are somewhat smaller than flavodoxin, fails to show any significant correlation between S_{axis}^2 parameters and the accessible surface area (*60*) or distance to the molecular surface (not shown) of the associated side chain. Indeed, the lack of obvious correlates with depth of burial combined with the high degree of heterogeneity in the distribution of S_{axis}^2 parameters is striking. These observations are qualitatively at odds with the so-called "surface molten" characteristic ascribed to condensed polypeptide chains (*66*). Interestingly, the correlation between depth of burial and degree of motional restriction, which is implied by the surface molten description of proteins, is seen for the first time in oxidized flavodoxin (C55A), albeit as a weak correlation. Figure 7 suggests that factors other than depth of burial dictate the amplitude of fast motion near the surface, while depth of burial becomes an increasingly dominant predictor of motional amplitude the further inside the protein the side chain resides. This is conceptually intuitive and follows from the obvious requirement in a closely packed polymer that cooperative motion is necessary to move any collection of atoms a significant distance. These data hint at the need to study the internal dynamics of even larger proteins to confirm and more fully characterize this dependency and its physical origins.

REFERENCES

1. Mayhew, S. G., and Tollin, G. (1992) *Chem. Biochem. Flavoenzymes 3*, 389−426.
2. Hoover, D. M., Drennan, C. L., Metzger, A. L., Osborne, C., Weber, C. H., Pattridge, K. A., and Ludwig, M. L. (1999) *J. Mol. Biol. 294*, 725−743.
3. Lostao, A., Gomez-Moreno, C., Mayhew, S. G., and Sancho, J. (1997) *Biochemistry 36*, 14334−14344.
4. Pueyo, J. J., Gomez-Moreno, C., and Mayhew, S. G. (1991) *Eur. J. Biochem. 202*, 1065−1071.
5. Draper, R. D., and Ingraham, L. L. (1968) *Arch. Biochem. Biophys. 125*, 802−808.
6. Ludwig, M. L., and Luschinsky, C. L. (1992) *Chem. Biochem. Flavoenzymes 3*, 427−466.
7. Rao, S. T., Shaffie, F., Yu, C., Satyshur, K. A., Stockman, B. J., Markley, J. L., and Sundaralingam, M. (1992) *Protein Sci. 1*, 1413−1427.
8. Genzor, C. G., Perales-Alcon, A., Sancho, J., and Romero, A. (1996) *Nat. Struct. Biol. 3*, 329−332.
9. Burkhart, B. M., Ramakrishnan, B., Yan, H., Reedstrom, R. J., Markley, J. L., Straus, N. A., and Sundaralingam, M. (1995) *Acta Crystallogr. D51*, 318−330.
10. Ludwig, M. L., Burnett, R. M., Darling, G. D., Jordan, S. R., Kendall, D. S., and Smith, W. W. (1976) in *Flavins Flavoproteins* (Massey, V., and William, C. H., Ed.) 5th ed., pp 393−404, Proceedings of International Symposia, Elsevier North-Holland, Inc., New York.
11. Watt, W., Tulinsky, A., Swenson, R. P., and Watenpaugh, K. D. (1991) *J. Mol. Biol. 218*, 195−208.
12. Muhandiram, D. R., Yamazaki, T., Sykes, B. D., and Kay, L. E. (1995) *J. Am. Chem. Soc. 117*, 11536−11544.
13. Wand, A. J., Urbauer, J. L., McEvoy R. P., and Beiber, R. J. (1996) *Biochemistry 35*, 6116−6125.
14. LeMaster, D. M., and Kushlan, D. M. (1996) *J. Am. Chem. Soc. 118*, 9255−9264.
15. Lee, A. L., Flynn, P. F., and Wand, A. J. (1999) *J. Am. Chem. Soc. 121*, 2891−2902.
16. Lee, A. L., and Wand, A. J. (2001) *Nature 411*, 501−504.
17. Fillat, M. F., Borrias, W. E., and Weisbeek, P. J. (1991) *Biochem. J. 280*, 187−191.
18. Ludwig, M. L., Pattridge, K. A., Metzger, A. L., Dixon, M. M., Eren, M., Feng, Y., and Swenson, R. P. (1997) *Biochemistry 36*, 1259−1280.
19. Tollin, G., and Edmondson, D. E. (1980) *Methods Enzymol. 69*, 392−406.
20. Fillat, M. F., Sandmann, G., and Gomez-Moreno, C. (1988) *Arch. Microbiol. 150*, 160−164.
21. Shaka, A. J., Barker, P. B., and Freeman, R. (1985) *J. Magn. Reson. 64*, 547−552.
22. Marion, D., Ikura, M., Tschudin, R., and Bax, A. (1989). *J. Magn. Reson. 85*, 393−399.
23. Cavanagh, J., and Rance, M. (1990) *J. Magn. Reson. 88*, 72−85.
24. Palmer, A. G., III, Cavanagh, J., Wright, P. E., and Rance, M. (1991) *J. Magn. Reson. 93*, 151−170.
25. Wijmenga, S., van Mierlo, C. P. M., and Steensma, E. (1996) *J. Biomol. NMR 8*, 319−330.
26. Wittekind, M., and Mueller, L. (1993) *J. Magn. Reson. 101*, 201−205.
27. Grzesiek, S., and Bax, A. (1992) *J. Am. Chem. Soc. 114*, 6291−6293.
28. Grzesiek, S., and Bax, A. (1992) *J. Magn. Reson. 96*, 432−440.
29. Jahnke, W., and Kessler, H. (1994) *J. Biomol. NMR 4*, 735−740.
30. Clubb, R. T., Thanabal, V., and Wagner, G. (1992) *J. Magn. Reson. 97*, 213−217.
31. Montelione, G. T., Lyons, B. A., Emerson, S. D., and Tashiro, M. (1992) *J. Am. Chem. Soc. 114*, 10974−10975.
32. Bax, A., Clore, G. M., and Gronenborn, A. M. (1990) *J. Magn. Reson. 88*, 425−431.
33. Uhrin, D., Uhrinova, S., Leadbeater, C., Nairn, J., Price, N. C., and Barlow, P. N. (2000) *J. Magn. Reson. 142*, 288−293.
34. Neri, D., Szyperski, T., Otting, G., Senn, H., and Wüthrich, K. (1989) *Biochemistry 28*, 7510−7516.
35. Wishart, D. S., Bigam, C. G., Yao, J., Abildgaard, F., Dyson, H. J., Oldfield, E., Markley, J. L., and Sykes, B. D. (1995) *J. Biomol. NMR 6*, 135−140.
36. Nirmala, N. R., and Wagner, G. (1988) *J. Am. Chem. Soc. 110*, 7557−7558.
37. Palmer, A. G., III, and Case, D. A. (1992) *J. Am. Chem. Soc. 114*, 9059−9067.
38. Kay, L. E., Torchia, D. A., and Bax, A. (1989) *Biochemistry 28*, 8972−8979.
39. Farrow, N. A., Muhandiram, R., Singer, A. U., Pascal, S. M., Kay, C. M., Gish, G., Shoelson, S. E., Pawson, T., Forman-Kay, J. D., and Kay, L. E. (1994) *Biochemistry 33*, 5984−6003.

40. Lee, L. K., Rance, M., Chazin, W. J., and Palmer, A. G., III (1997) *J. Biomol. NMR 9*, 287−298.
41. Overhauser, A. W. (1953) *Phys. Rev. 92*, 411.
42. Freeman, R., Hill, H. D. W., and Kaptein, R. (1972) *J. Magn. Reson. 7*, 82−98.
43. Williams, W. D., Seymour, E. F. W., and Cotts, R. M. (1978) *J. Magn. Reson. 31*, 271−282.
44. Lipari, G., and Szabo, A. (1982) *J. Am. Chem. Soc. 104*, 4546−4559.
45. Lipari, G., and Szabo, A. (1982) *J. Am. Chem. Soc. 104*, 4559−4570.
46. Cornilescu, G., and Bax, A. (2000) *J. Am. Chem. Soc. 122*, 10143−10154.
47. Mantsch, H. H., Saito, H., and Smith, I. C. P. (1977) *Prog. NMR Spectrosc. 11*, 211−271.
48. Steensma, E., Heering, H. A., Hagen, W. R., and Van Mierlo, C. P. M. (1996) *Eur. J. Biochem. 235*, 167−172.
49. Stockman, B. J., Krezel, A. M., Markley, J. L., Leonhardt, K. G., and Straus, N. A. (1990) *Biochemistry 29*, 9600−9609.
50. Stockman, B. J., Reily, M. D., Westler, W. M., Ulrich, E. L., and Markley, J. L. (1989) *Biochemistry 28*, 230−236.
51. Tjandra, N., Kuboniwa, H., Ren, H., and Bax, A. (1995) *Eur. J. Biochem. 230*, 1014−1024.
52. Schurr, J. M., Babcock, H. P., and Fujimoto, B. S. (1994) *J. Magn. Reson., Ser. B 105*, 211−224.
53. Flynn, P. F., Bieber Urbauer, R. J., Zhang, H., Lee, A. L., and Wand, A. J. (2001) *Biochemistry 40*, 6559−6569.
54. Zhang, P., Dayie, K. T., and Wagner, G. (1997) *J. Mol. Biol. 272*, 443−455.
55. Dellwo, M. J., and Wand, A. J. (1989) *J. Am. Chem. Soc. 111*, 4571−4578.
56. Lee, A. L., Urbauer, J. L., and Wand, A. J. (1997) *J. Biomol. NMR 9*, 437−440.
57. Kay, L. E., Muhandiram, D. R., Farrow, N. A., Aubin, Y., and Forman-Kay, J. D. (1996) *Biochemistry 35*, 361−368.
58. Constantine, K. L., Friedrichs, M. S., Wittekind, M., Jamil, H., Chu, C.-H., Parker, R. A., Goldfarb, V., Mueller, L., and Farmer, B. T., II (1998) *Biochemistry 37*, 7965−7980.
59. Gagne, S. M., Tsuda, S., Spyracopoulos, L., Kay, L. E., and Sykes, B. D. (1998) *J. Mol. Biol. 278*, 667−686.
60. Mittermaier, A., Kay, L. E., and Forman-Kay, J. D. (1999) *J. Biomol. NMR 13*, 181−185.
61. Nicholls, A., Sharp, K. A., and Honig, B. (1991) *Proteins: Struct., Funct., Genet. 11*, 281−296.
62. Lee, A. L., Kinnear, S. A., and Wand, A. J. (2000) *Nat. Struct. Biol. 7*, 72−77.
63. Lostao, A., Harrous, M. E., Daoudi, F., Romer, A., Parody-Morreales, A., and Sancho, J. (2000) *J. Biol. Chem. 275*, 9518−9526.
64. Li, Z., Raychaudhuri, S., and Wand, A. J. (1996) *Protein Sci. 5*, 2647−2650.
65. Steensma, E., Nijman, M. J., Bollen, Y. J., de Jager, P. A., van den Berg, W. A., van Dongen, W. M., and van Mierlo, C. P. (1998) *Protein Sci. 7*, 306−317.
66. Zhou, Y., Vitkup, D., and Karplus, M. (1999) *J. Mol. Biol. 285*, 1371−1375.
67. Koradi, R., Billeter, M., and Wüthrich, K. (1996) *J. Mol. Graphics 14*, 29−32.

BI011073D